Cirrus Cloud Properties Derived from High Spectral Resolution Infrared Spectrometry during FIRE II. Part III: Ground-Based HIS Results

A. D. COLLARD, S. A. ACKERMAN, W. L. SMITH, X. MA, H. E. REVERCOMB, R. O. KNUTESON, AND S.-C. LEE

Cooperative Institute for Meteorological Satellite Studies, Space Science and Engineering Center, University of Wisconsin-Madison, Madison, Wisconsin

(Manuscript received 19 July 1994, in final form 8 December 1994)

ABSTRACT

During FIRE II, cirrus clouds were observed in the wavelength range 3–19 μm with two High Resolution Interferometer Sounders as described in the Part I companion paper. One, known as AC-HIS, was mounted on the NASA ER-2 aircraft in order to look down on the clouds; these results are described in the Part II companion paper. The other, GB-HIS, also known as the Atmospheric Emitted Radiance Interferometer (AERI), was ground based. The AERI observations have been simulated, assuming scattering from spherical ice particles, using a single-layer doubling model for the cloud, for two atmospheric windows at 700–1250 and 2650–3000 cm^{-1}. The second of these windows is affected by scattered sunlight, which has been included in the calculations. The sensitivity of the cloud signal to quantities such as the ice water path (IWP) and effective radius (r_{eff}) have been determined. Using the cloud model, best fits have been derived for IWP and r_{eff}, for both windows individually and together. Possible errors in these derivations have been investigated.

1. Introduction

The uplooking GB-HIS spectrometer (called the AERI—Atmospheric Emitted Radiance Interferometer) observes at an unapodised spectral resolution of approximately 0.5 cm^{-1} over two bands in the infrared. Band I covers the range 500–1800 cm^{-1}, while band II covers 1800–3000 cm^{-1}. For further details of the characteristics of this instrument and its role in the FIRE II experiment see Part I of this series [Smith et al. (1995) and Revercomb et al. (1993).]

Observations of thin cirrus clouds were made on various days throughout the First ISCCP Regional Experiment-Phase II (FIRE II) period. Specific periods for study were chosen based on having a homogeneous, single cirrus cloud layer and a close clear-sky observation.

The spectral region observed by the GB-HIS is shown in Fig. 1. Emission features due to CO_2, H_2O, and O_3 are apparent. Also, there are two window regions where the atmospheric transmission is greater than 90%. In these regions the effect of cloud is most obvious. The wavelength intervals from 760–1235 cm^{-1} (excluding the ozone band at 1000–1067 cm^{-1}), hereinafter referred to as "window 1," and from 2480–2950 cm^{-1} (window 2) are used for the retrieval of cloud properties.

Corresponding author address: Dr. William L. Smith, CIMSS, Space Science and Engineering Center, University of Wisconsin-Madison, 1225 West Dayton St., Madison, WI 53706.

As noted by Smith et al. (1993), the emissivities of cirrus clouds vary with wavenumber in the window 1 region. Smith et al. used this structure to infer microphysical properties of the clouds. This paper extends the Smith et al. analysis to the band II region. As will be explained later, observed radiances in window 2 arise from a physical process different than that associated with window 1. As a consequence, the cloud emissivity is not as useful a quantity, in this case, for the specification of cloud microphysical properties and as a result is not used in this paper. Here we attempt to derive cloud microphysical properties directly from the GB-HIS radiance observations, using a doubling radiative transfer model and a simple retrieval scheme. These are described below with an investigation of the effect of some of the unknowns and approximations that may affect the conclusions drawn.

2. The radiative transfer model

The analysis of these data uses a single-layer doubling model (Wiscombe 1976a,b) for the clouds with radiances and transmittances of the gaseous atmosphere calculated using FASCODE (Anderson and Chetwynd 1992). Emission from the surface can also affect the observed downwelling radiance through reflection by the clouds. This effect, which is generally more than an order of magnitude less than direct emission from the clouds, is included by assuming that the surface emits as a blackbody.

In this model the atmosphere is divided into three layers corresponding to the regions below, in, and

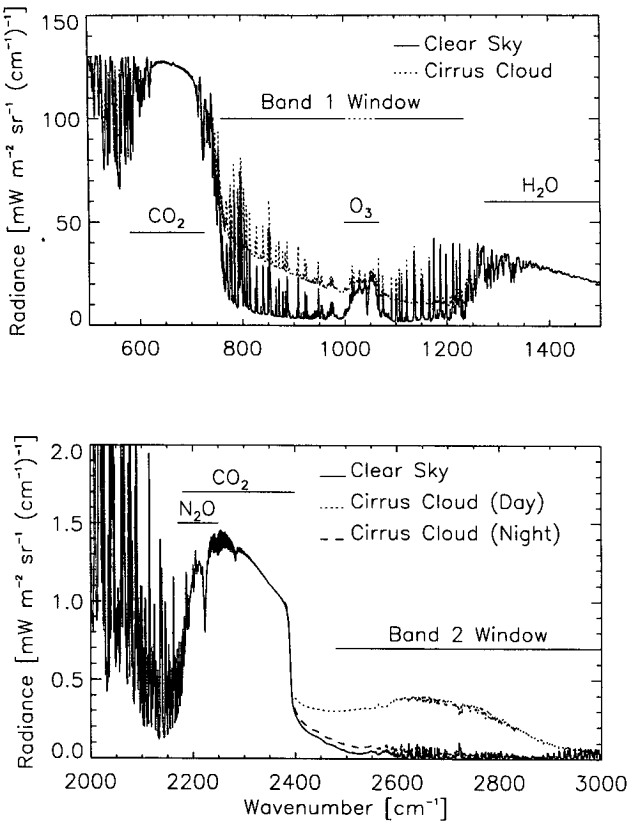

FIG. 1. Simulated GB-HIS observations for a clear-sky case and for the case of a high thin cirrus cloud in daylight. The effect of the cloud can be most readily seen in the window regions between 760 and 1250 cm^{-1} (window 1) and 2380 and 3000 cm^{-1} (window 2). Broad emission features due to H_2O, CO_2, and O_3 can be seen, and even in the band I window region spectral lines (mostly water) are apparent.

above the clouds (Ackerman and Knuteson 1993). FASCODE is used to calculate the transmissions and emergent intensities of each layer. The transmissions are assumed to obey the monochromatic product rule, although they are the average over the GB-HIS spectral response function. This approximation, while not generally valid, particularly in regions of significant gaseous line absorption, is satisfactory in the window regions where the transmissions do not vary greatly across a GB-HIS spectral element.

To allow for uncertainties in the assumed atmospheric state and in the spectroscopy employed in the radiative transfer model, use is made of the "gamma correction" as described by Smith et al. (1993). This correction is a multiplicitive factor applied equally to the optical depths of each layer in the atmosphere and for each observation channel. It is determined by comparing a model run and a clear-sky observation, usually close in time to the cloud observation. The effect of the gamma correction on the retrieved cloud parameters is shown in section 6.

The cloud particle optical properties are calculated using Mie theory for ice spheres in terms of the extinction, the single scattering albedo, and the asymmetry parameter. The latter is converted into a phase function via the Henyen–Greenstein function. A Hansen size distribution (Hansen 1971) is assumed, as given in Eq. (1),

$$n(r)dr = cr^{(1-3b)/b} \exp(-r/r_{\text{eff}}b)dr, \quad (1)$$

where $n(r)$ is the number of particles of radius r, r_{eff} is the effective radius, b is a variance term, and c is a normalization constant. Reasonable variation in the value of b has a small effect on the cloud radiative properties and is assumed to be 0.25.

The approximation to ice spheres, instead of the multitude of possible particle shapes typical of a cirrus cloud, may cause the retrieved parameters to be inaccurate and/or inconsistent. The effects of particle shape and multimodal particle size distributions are investigated in sections 7 and 8.

For the shorter wavelength window the contribution from the solar radiation is significant. Therefore, the solar source term is included in the model to simulate zenith (as with GB-HIS) or nadir (as with AC-HIS) observations. The solar irradiance used is that of Smith and Gottlieb (1974).

3. Retrieval procedures

A simple retrieval routine is used to find the ice water path and effective radius of the cirrus cloud particles that best fit the downwelling spectral radiance observations. The radiative transfer equations are put into a linear form in order to facilitate the cloud retrieval process.

Fitting parameters are chosen by considering the simplified situation of a thin cloud entirely above the gaseous absorption. In this case the radiance, I_{obs}, observed by an uplooking instrument is given by

$$I_{\text{obs}} = I_{\text{clear}} + I_{\text{cloud}} e^{-\tau}, \quad (2)$$

where I_{clear} is the emission from the atmosphere below cloud level (assumed to be the same as that of the clear atmosphere) and τ is the optical depth of the atmosphere below the cloud base. Therefore,

$$\log_e I_{\text{cloud}} = \log_e(I_{\text{obs}} - I_{\text{clear}}) + \tau. \quad (3)$$

For the case of a thin cloud the radiance from the cloud will be proportional to the quotient of the ice water path (IWP) and the effective radius (r_{eff}) so that $I_{\text{cloud}} \propto \text{IWP}/r_{\text{eff}}$. Here, this relationship is generalized to $I_{\text{cloud}} = C_1(\text{IWP})^{\alpha}(r_{\text{eff}})^{\beta}$, where α and β are, for a given wavelength, unknown constants and C_1 is a function of cloud temperature and solar irradiance. Equation (3) becomes

$$\log_e(I_{\text{obs}} - I_{\text{clear}}) = \alpha \log_e(\text{IWP}) + \beta \log_e(r_{\text{eff}}) + C_2, \quad (4)$$

where $C_2 = C_1 - \tau$ and is constant at a given wavelength.

The constant C_2 can be removed by determining IWP and r_{eff} relative to a known reference model calculation, which produces a radiance I_{ref}. This gives

$$\log_e[(I_{\text{obs}} - I_{\text{clear}})/(I_{\text{ref}} - I_{\text{clear}})] = \alpha \log_e(\text{IWP}') + \beta \log_e(r'_{\text{eff}}), \quad (5)$$

where $\text{IWP}' = \text{IWP}/\text{IWP}_{\text{ref}}$ and $r'_{\text{eff}} = r_{\text{eff}}/(r_{\text{eff}})_{\text{ref}}$. Equation (4) is thus a linear equation in α and β of the form $\mathbf{y} = \mathbf{K}\mathbf{x}$. The values of α and β are determined by running the forward model for a reference case and cases with IWP or r_{eff} slightly perturbed. The problem is now solved using the standard retrieval method of Rodgers (1976) where the retrieved state vector $\hat{\mathbf{x}}$ (in this case, the ice water path and the effective radius) is determined by

$$\hat{\mathbf{x}} = \mathbf{x}_0 + \mathbf{S}_0\mathbf{K}^{\mathrm{T}}(\mathbf{K}\mathbf{S}_0\mathbf{K}^{\mathrm{T}} + \mathbf{S}_\epsilon)^{-1}(\mathbf{y} - \mathbf{K}\mathbf{x}_0), \quad (6)$$

where $\mathbf{y}$ is the vector of observations, $\mathbf{K}$ is the "weighting function" matrix (consisting of the α and β for each wavenumber), $\mathbf{S}_\epsilon$ is the observational error covariance matrix, and $\mathbf{x}_0$ and $\mathbf{S}_0$ are the a priori state vector and its associated error covariance matrix.

To allow for the nonlinearities due to the various approximations employed in this method, Eq. (6) is iterated to convergence.

The functions $\log_e[(I_{\text{obs}} - I_{\text{clear}})/(I_{\text{ref}} - I_{\text{clear}})]$ and $(I_{\text{obs}} - I_{\text{clear}})$ can also be used to quantitatively display the effect of varying cloud microphysical properties. The latter of these is also referred to here as the "cloud forcing," although note the multiplicitive factor due to transmission of the subcloud atmosphere and that this refers to a directional radiance rather than a flux.

4. Sensitivity studies for ice water path and effective radius

Figure 2 shows the scattering properties for ice spheres as calculated using Mie theory for various effective radii. Structure is apparent in the shapes of these functions. It would thus appear that effective radii may be retrievable from the shapes of the cloud forcing functions, $I_{\text{obs}} - I_{\text{clear}}$.

Figure 3 illustrates this further by indicating how $I_{\text{cloud}} - I_{\text{clear}}$ is changed by varying r_{eff} for the case of a high cloud with the parameters described for 26 November 1991 in Table 1a. It is apparent that the spectroscopic variation of $(I_{\text{obs}} - I_{\text{clear}})$ is significant both across window 1 and between windows 1 and 2. For thin clouds the effect of changing the ice water path while keeping r_{eff} fixed is seen to change only the magnitude rather than the shape of $(I_{\text{obs}} - I_{\text{clear}})$. For thick clouds the shape of $(I_{\text{obs}} - I_{\text{clear}})$ changes in both windows, consistent with the increased importance of scattering in window 1 and absorption in window 2 (see below), although for window 1 this effect is no larger than about 10%.

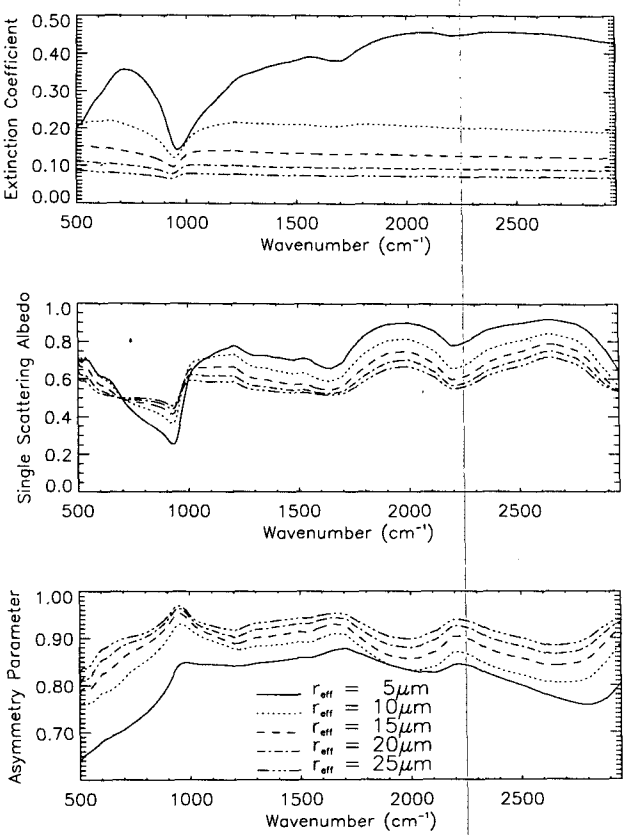

FIG. 2. Spectral properties of ice spheres for the GB-HIS wavenumber interval for five different size distributions. Note the increasing structure with decreasing effective particle size and the relatively flat functions in the window 2 region compared to window 1.

Figures 4a and 4b illustrate the effect of changing IWP and r_{eff} at typical wavelengths in each window. The different radiative properties of the clouds in the two windows are apparent. In window 1 the clouds' signal is due almost entirely to thermal emission. Therefore, the cloud forcing increases with IWP until it reaches an asymptote where the cloud is totally opaque and the signal is a maximum. Window 2, as mentioned above, is dominated by solar scattering, and the cloud forcing thus increases with IWP as the number of particles scattering solar radiation toward the instrument rises. Eventually, the opacity of the cloud increases to the extent that sunlight is prevented from reaching the instrument, and the signal is reduced until only the small contribution of thermal emission remains at high IWP.

Simple geometric considerations indicate that the quotient $\text{IWP}/r_{\text{eff}}$ is proportional to the optical depth of the clouds. Figure 5 indicates how the cloud forcing is related to this quantity for various effective radii. The correlation of $I - I_{\text{clear}}$ with $\text{IWP}/r_{\text{eff}}$ in window 1 is

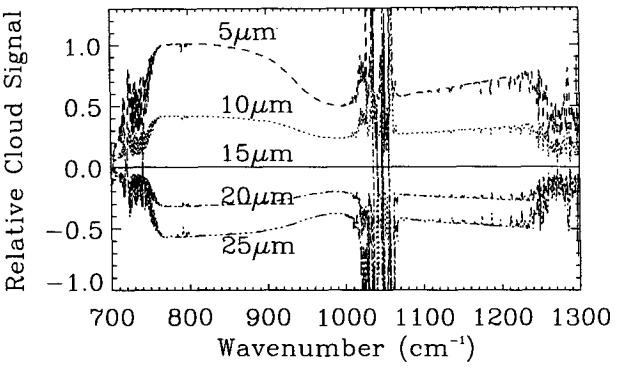

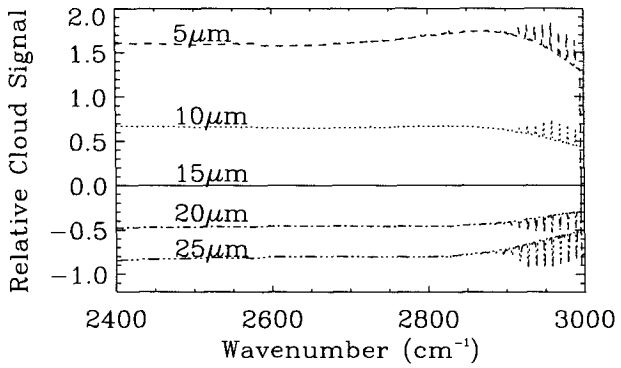

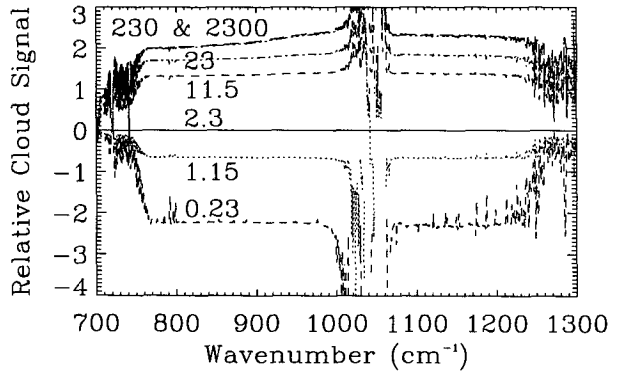

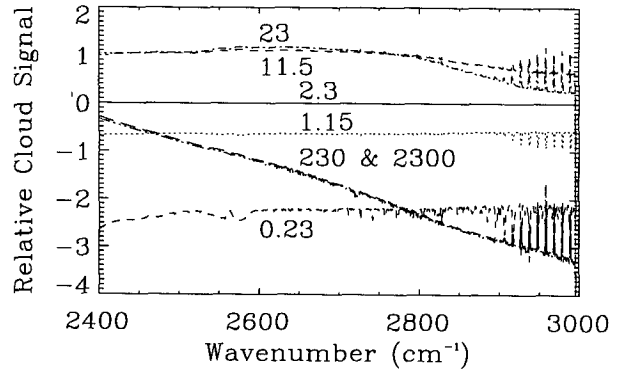

good (to first order, information on particle size can be derived from second-order variations affecting the shape of the cloud spectrum), while for window 2 this parameter does not appear to be useful, which is consistent with the greater importance of particle scattering properties in this window.

5. Observations

The primary observations employed were made with the GB-HIS (i.e., the AERI) instrument from the FIRE II site at Coffeyville, Kansas, in November and December 1991. Use was also made of NCAR Cross-chain linked Atmospheric Sounding System (CLASS) radiosondes for derivation of the temperature and H_2O volume mixing ratio profiles used in the model. Cloud base and top heights are obtained with a CO_2 Doppler lidar operated by NOAA (Intrieri et al. 1993; Uttal et al. 1995). The lidar operates at 10 μm (i.e., in the middle of the GB-HIS band 1), and thus the cloud heights derived are particularly consistent with GB-HIS use.

The observations to be studied in detail are chosen on the basis of a number of criteria. First, to simplify the analysis, observations of a single layer of cirrus cloud with an apparently homogeneous structure are chosen. Second, a radiosonde observation and an observation of a clear-sky radiance both close in time to the AERI observation are desirable.

The determination of a "clear sky" is somewhat ambiguous as very thin clouds may be detected by the CO_2 lidar, which have a totally negligible effect on the observed radiances.[1] The clear-sky observations are thus

[1] Simple calculations show that for a cloud with a temperature of 230 K its emission becomes significant relative to the instrumental and spectroscopic noise when its optical depth is above 0.02. This corresponds to a value of IWP/r_{eff} of around 0.02 g m^{-2} μm^{-1}.

FIG. 3a. The effect on the radiance from a high thin cirrus of changing the effective radius of the cloud particles, keeping the ice water path fixed (2.3 g m^{-2}). The ordinate, $\log_e[(I - I_{\text{clear}})/(I - I_{\text{clear}})_{15\,\mu\text{m}}]$, is the logarithm of the cloud forcing divided by a base model. This essentially removes the effect of transmission of the lower atmosphere. At the edges of the window regions and in the ozone absorption feature around 1040 cm^{-1} there is contamination due to absorption being significant in the cloud layer and above. It may be seen that the magnitude of the cloud forcing varies with wavenumber across the band I window and between the two windows. From this we may conclude that there is size information to be gained from the spectral variation in the cloud response in these regions.

FIG. 3b. As in Fig. 3a except the curves are for different ice water paths (in g m^{-2}) and are plotted relative to the signal for a cloud with IWP = 23 g m^{-2}. The effective radius is kept fixed at 15 μm. For thin clouds the curves are spectrally flat, from which we may conclude that only the magnitude and not the shape of the cloud forcing is dependent on the ice water path in this case. In both windows thicker clouds introduce some extra spectral structure. For the band I window this is small (~10%) and is probably due to the increased influence of scattering. In the band II window the effect is larger and probably a direct result of the transmission of the cloud becoming more important (see text).

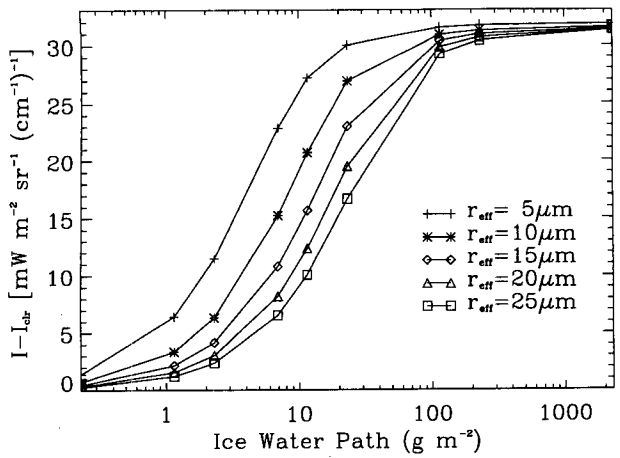

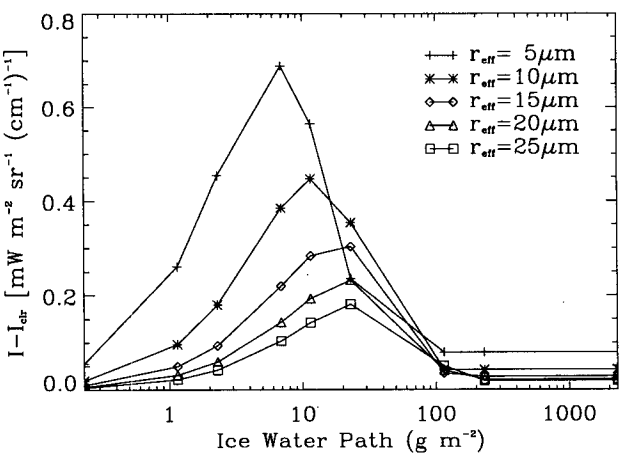

FIG. 4a. Variation of the cloud forcing (multiplied by the transmission of the lower atmosphere, about 0.9) with ice water path and effective radius for a typical model high thin cirrus cloud at 800 cm^{-1}, i.e., in the thermal emission dominated band I window. The cloud forcing increases monotonically with ice water path until the cloud is essentially opaque and the signal is a maximum.

FIG. 4b. As in Fig. 4a except for 2600 cm^{-1} (window 2). The calculations assume incident sunlight, and the result is that for small ice water paths the cloud signal increases with IWP as more sunlight is scattered toward the instrument. At larger IWP the opacity of the cloud reduces the scattered sunlight reaching the GB-HIS until only the small thermal emission term remains as the cloud becomes opaque.

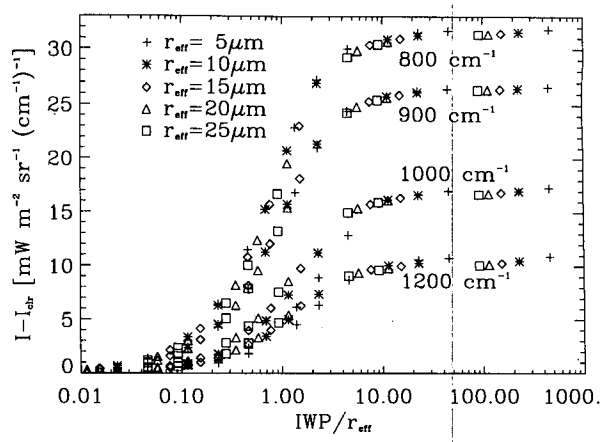

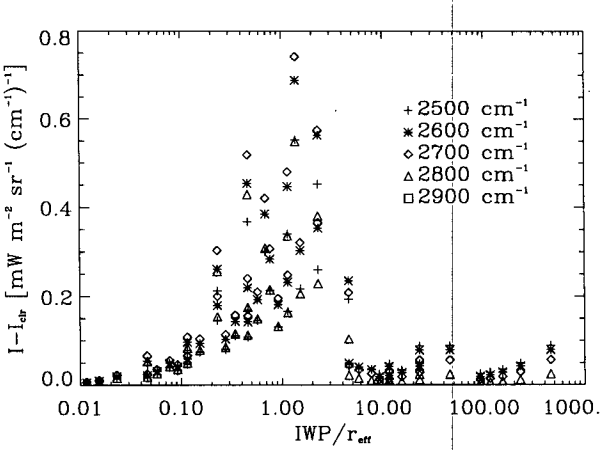

FIG. 5a. As in Fig. 4a except the cloud forcing is now plotted vs IWP/r_{eff}. This quotient is proportional to the optical depth of the cloud. Four wavenumbers are plotted: (top to bottom) 800, 900, 1000, and 1100 cm^{-1}. It can be seen that correlation between IWP/r_{eff} and $I - I_{clear}$ is good in all cases.

FIG. 5b. As in Fig. 5a except for five window 2 wavenumbers. The correlation is not good, indicating the more complicated radiative processes in this window. Note that, unlike Fig. 5a, the symbols refer to different frequencies, not different particle sizes.

chosen on the basis of a combination of lidar observations, visual logs made by GB-HIS operators, and variations of the observed radiances with time. It shall be seen that the gamma-corrected radiances and transmittances produced here appear to be adequate for the cloud parameter retrieval process.

One time period was thus chosen for study, between 1800 and 1900 UTC 26 November 1991. This is also useful as r_{eff} and IWP have independently been derived by Intrieri et al. (1993) using a combination of microwave and infrared radar/lidar. Further information on the observation period chosen is given in Table 1a. The clear-sky observation was made at 1722 UTC.

A second, though less satisfactory, period is also analyzed. This is 1645–1839 UTC 5 December 1991; details are given in Table 1b.

TABLE 1a. Details of the observations used from 26 November 1991 in this analysis as cloud base/cloud top value.

Time (UTC)	Height (km) from NOAA lidar	Temperature (K) from 1716 UTC NCAR CLASS sonde	Pressure (mb)
18.01	8.7/10.5	228.68/213.99	324.2/245.3
18.12	8.5/10.4	230.47/213.83	334.0/249.3
18.22	8.5/10.4	230.47/213.83	334.0/249.3
18.32	8.7/10.5	228.68/213.99	324.2/245.3
18.43	8.3/10.7	231.93/215.55	344.0/237.6
18.53	8.3/10.5	231.93/213.99	344.0/245.3

TABLE 1b. Details of the observations used from 5 December 1991 in this analysis as cloud base/cloud top value.

Time (UTC)	Height (km) from NOAA lidar	Temperature (K) from 1715 UTC NCAR CLASS sonde	Pressure (mb)
16.45	11.2/12.5	219.87/210.02	227.9/185.3
17.07	10.2/12.1	227.58/212.16	265.4/197.7
17.40	10.5/12.3	225.76/210.34	253.7/191.4
18.07	10.2/12.4	227.58/209.96	265.4/188.3
18.18	10.2/12.4	227.58/209.96	265.4/188.3
18.28	10.2/12.2	227.58/211.25	265.4/194.5
18.39	10.2/12.3	227.58/210.34	265.4/191.4

It should be noted that at night the signal due to high thin cirrus clouds in the shortwave window was too low to be usable. Therefore, no nighttime observations are considered in this paper.

6. Results from GB-HIS observations

The initial fitting investigations employ the GB-HIS observations at 1832 UTC 26 November. The results are shown in Table 2. Six fitting runs are displayed: two each for window 1 only, window 2 only, and both windows together, with each window being fitted using models employing and not employing the gamma correction. The values of the parameters derived using the gamma correction are very similar to those derived without, but a large difference is found between the values of r_{eff} and IWP using the different windows.

The significance of (a) the gamma functions and (b) the use of the different windows for fitting can be appreciated in Figs. 6 and 7. Figure 6 compares a window 1 fit with and without the gamma function. It is obvious that, while both fits return similar parameter values, the fit without the correction is far less convincing.

Figure 7 shows a large error in the radiances of the other window when fits are made in one window only. The both-window fit is almost as good as the window 2 fit in band II, but in band I, the spectral variation of the cloud signal is not well matched, and the window 1 fit is clearly superior.

A comparison between the values of IWP/r_{eff} for each case investigated reveals that this value is approximately the same for the "both windows" and "window 1 only" fit, but is markedly different when window 2 is used. This inconsistency between the two regions may, of course, be a phenomenon peculiar to the time of the observation. Hence, the same analysis is now carried out for other times in the periods discussed above. The results of these (for the both windows and window 1 only cases) are presented in Tables 3a and 3b. The differences between the two fits and the absolute effective radii derived are consistent for all observations.

It should be noted that the values for IWP and r_{eff} obtained from both window fits are somewhat inaccurate. All that can safely be inferred is that the apparent effective radius is greater than about 30 μm, as particles larger than this do not greatly affect the spectral structure. The quotient IWP/r_{eff} can, however, be derived with reasonable accuracy, and as a result the errors in r_{eff} and IWP are highly correlated.

TABLE 2. Fits to each of the windows and both windows observed by GB-HIS at 1832 UTC 26 November 1991.

	Without gamma			With gamma		
	IWP	r_{eff}	IWP/r_{eff}	IWP	r_{eff}	IWP/r_{eff}
Window 1	8.599	12.934	0.665	8.375	17.316	0.484
Window 2	57.901	40.244	1.439	60.867	43.471	1.400
Both windows	31.192	46.495	0.671	22.016	44.812	0.491

7. Fitting to artificial cylindrical clouds

The differences between the single-band and the two-band fits may result from the assumption of spherical ice particles. To test this, GB-HIS observations were simulated using single scattering properties of cylindrical ice particles. Figure 8 shows the results of a "retrieval" of r_{eff} and IWP to a model run calculated assuming a distribution of cylindrical ice particles. The "real" r_{eff} for the distribution is, of course, somewhat illdefined but it may most sensibly be defined as the radius of a sphere with the same cross-sectional area as that of a randomly oriented cylinder. Using this definition, the r_{eff} used in this simulation is 16.33 μm with an ice water path of 2.3 gm^{-2} (which gives a value for IWP/r_{eff} of 0.141). The results of attempting to fit these "observations" using the ice sphere model are given in Tables 4a (for daytime) and 4b (for night).

These fits show a similar quantitative behavior to those obtained above using the real observations in that

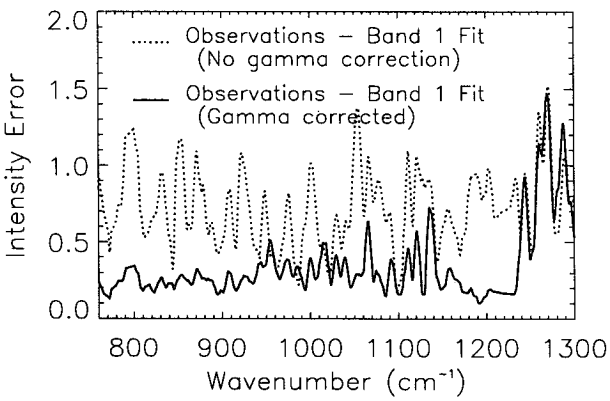

FIG. 6. The fitting error (observed minus fitted intensity) in window 1 for the case of 1832 UTC 26 November 1991. For clarity, the function shown is the square root of the result of smoothing the square of the true fitting error. As can be seen, the use of the gamma correction significantly reduces the observation–fit discrepancy.

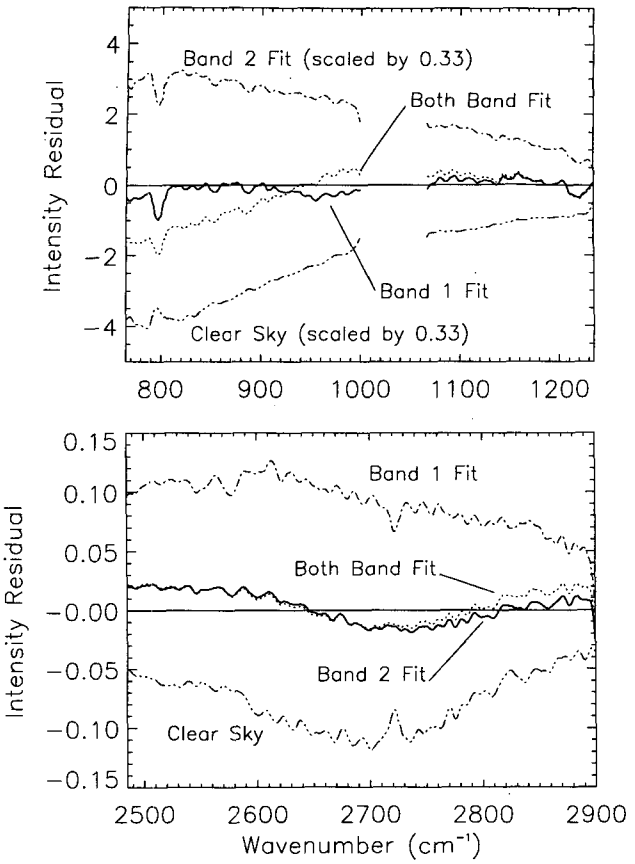

FIG. 7. A comparison of the intensity residuals (fitted minus observed intensity) for retrievals using window 1 only, window 2 only, and both windows together. Also shown is the clear sky − observed difference. The curves are smoothed to 5 cm^{-1} resolution for clarity.

markedly different values of the parameters are required to fit window 1 and both windows together. One may thus conclude that the discrepancies between the two fits in the observations may be related to the crude representation of the shapes used. While large differences exist in the retrievals of IWP and r_{eff}, the spherical particle assumption does a reasonable job of retrieving the ratio (IWP/r_{eff}), which is proportional to cloud optical depth.

The simulated nighttime investigations are important, as they provide a test where the radiative processes

TABLE 3a. Fits to the observations used from 26 November 1991.

Time (UTC)	Window 1			Both windows		
	r_{eff}	IWP	IWP/r_{eff}	r_{eff}	IWP	IWP/r_{eff}
1801	21.275	11.311	0.532	55.704	29.952	0.538
1812	14.430	2.176	0.151	73.773	11.172	0.151
1822	15.799	2.451	0.155	127.272	20.072	0.158
1843	13.544	7.706	0.569	33.944	18.787	0.553
1853	17.176	6.974	0.406	73.372	31.365	0.427

TABLE 3b. Fits to the observations used from 5 December 1991.

Time (UTC)	Window 1			Both windows		
	r_{eff}	IWP	IWP/r_{eff}	r_{eff}	IWP	IWP/r_{eff}
1645	11.269	2.137	0.190	13.748	2.523	0.184
1707	19.713	1.830	0.093	29.213	2.728	0.093
1740	13.645	1.850	0.136	21.004	2.785	0.133
1807	18.114	3.366	0.186	36.933	6.937	0.188
1818	16.334	3.788	0.232	37.406	8.793	0.235
1828	15.605	4.292	0.275	25.787	7.060	0.273
1839	18.289	5.137	0.281	39.657	11.367	0.287

in the two windows are the same (it is, of course, not possible in reality to do nighttime retrievals using both bands because of the low thermal emission signal in window 2). It should thus be noted that the results are similar in both daytime and nighttime cases.

8. Fitting bimodal distributions

The analysis performed assumes at present only one particle-size mode. To investigate the effect of bimodal distributions, a test scenario was set up with a small particle mode with r_{eff} = 5 μm and b = 0.03 and a large-particle mode with r_{eff} = 100 μm and b = 0.05. The particle number density for the small mode was set to 444 times that for the large mode so that the total

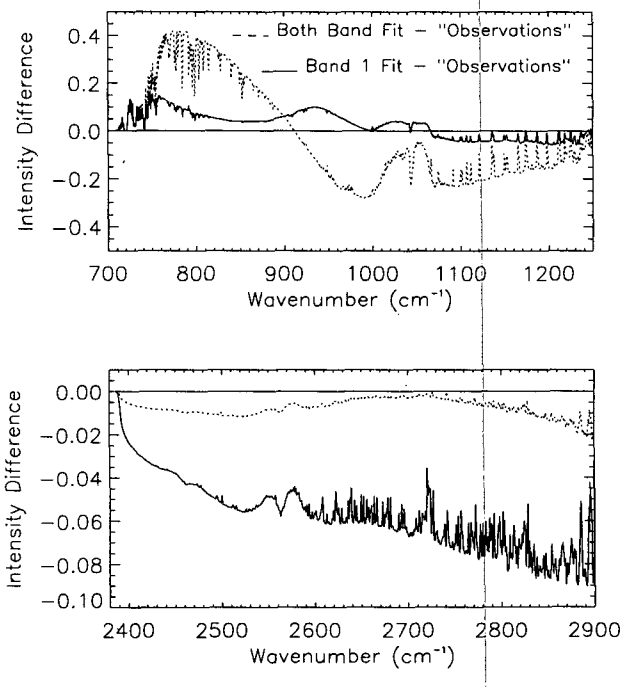

FIG. 8. A comparison of fits to an artificial observation produced assuming a distribution of cylindrical particles with effective radius 16.33 μm and an IWP of 2.3 g m^{-2}. As with the real observations, a consistent fit for window 1 and both windows is not possible.

TABLE 4a. Fits to simulated observations of clouds made up of ice cylinders in the daytime.

	IWP (g m^{-2})	r_{eff} (μm)	IWP/r_{eff}
Window 1	1.1983	9.37	0.128
Window 2	0.5957	4.45	0.134
Both windows	0.6486	4.68	0.134

cross-sectional areas of the two modes are approximately equal and the combined effective radius is 48.50 μm. This distribution is shown in Fig. 9.

Artificial observations are then produced using the cloud characteristics described with varying ice water paths. Results are summarized in Table 5.

It can be seen immediately that the derived effective radii are significantly smaller than truth. The optical depths (approximately proportional to IWP/r_{eff}) are generally quite close, resulting in the IWPs being significantly smaller also. This is not surprising when one considers that, at these wavelengths, the optical properties of smaller ice spheres vary most with size (as is apparent from Fig. 2), and as a result the average properties of a 5-μm and a 100-μm particle are going to resemble a 10-μm particle rather than one with a radius of 50 μm.

To illustrate this further, in Fig. 10 the extinction coefficients of various monomodal distributions are plotted, normalized to unity at 900 cm^{-1}. Also plotted is the extinction coefficient for the bimodal distribution described above, similarly normalized. The shape of the curve is closest to that for 5 or 10 μm particles.

Inspection of the fitted curves indicates that for certain cases the two-window retrievals fit the shape of the window 1 signal reasonably well. This is particularly true for very small and very large values of IWP/r_{eff}. In other cases, however, errors comparable with those seen in the observations are apparent. We may thus conclude that the possible existence of multiple particle size modes may be responsible for some or all of the inconsistencies seen in the observations. It should be noted that for this to be the case there must be many more smaller particles than larger ones. The ratio of number densities must be greater than the square of the ratio of the effective radii of the two modes; however, this scenario would still result in the smaller mode containing less ice than the larger mode.

TABLE 4b. Fits to simulated observations of clouds made up of ice cylinders at night.

	IWP (g m^{-2})	r_{eff} (μm)	IWP/r_{eff}
Window 1	1.1937	9.35	0.128
Window 2	0.6670	4.52	0.148
Both windows	0.8349	5.75	0.145

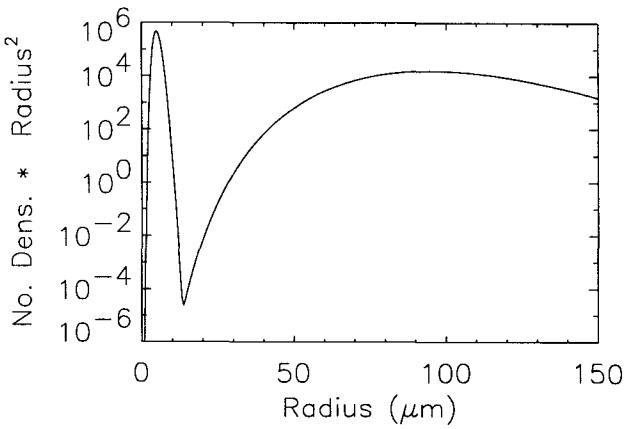

FIG. 9. The bimodal size distribution used in the investigations. The two distributions have effective radii of 5 and 100 μm, with a combined r_{eff} of 48.5 μm.

9. The effect of errors in clear-sky radiative transfer

In this section the effect of inaccurate knowledge of the clear-sky radiance and transmittance is investigated. To this end, radiative transfer calculations based on adjacent radiosonde profiles are compared, and the effect of the differences on the derived parameters is examined.

The time period used is that around the cirrus observations at 1830 UTC 26 November 1991. The radiosonde times are 1412, 1725, and 2330 UTC, which are from 0812 until 1730 local time. The skies were clear at the time of the first two observations, while at 2025 there were cirrus clouds overhead, and there was a mixed cloud layer at 2330.

Figure 11 shows the differences in the clear-sky radiances relative to the 2330 case for window 1. Differences in radiances between adjacent sondes are as large

TABLE 5. Fits to artificial clouds with the bimodal particle-size distribution described in the text with the fitting routine assuming a monomodal distribution.

	IWP	r_{eff}	IWP/r_{eff}
Actual IWP = 2.3 (g m^{-2}) (IWP/r_{eff} = 0.0474)			
Window 1	0.460	10.533	0.0436
Window 2	0.276	7.351	0.0375
Both windows	0.391	9.091	0.0430
Actual IWP = 23.0 (g m^{-2}) (IWP/r_{eff} = 0.474)			
Window 1	4.250	9.346	0.455
Window 2	1.840	6.620	0.278
Both windows	3.452	8.995	0.384
Actual IWP = 230 (g m^{-2}) (IWP/r_{eff} = 4.74)			
Window 1	44.30	10.497	4.22
Window 2[a]	—	—	—
Both windows	92.63	22.027	4.21

[a] Does not converge after ten iterations.

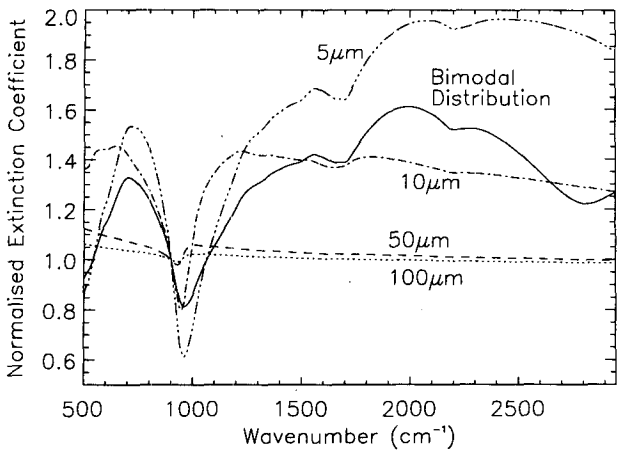

FIG. 10. The spectral variation of the extinction coefficient of the bimodal particle size distribution used in the text compared to various monomodal distributions. Each curve has been scaled to unity at 900 cm^{-1} to aid comparison. It should be noted that, whereas the effective radius of the bimodal distribution is 50 μm, the spectral variation of the extinction coefficient is more similar to monomodal distributions with effective radii of 5 or 10 μm.

as 7 mW m^{-2} sr^{-1} $(cm^{-1})^{-1}$ and have spectral structure similar to that displayed by cirrus clouds. The majority of the variation in the window region is due to changes in the emission from the water vapor continuum (also discussed in the next section). Window 2 differences are far less significant.

The same comparison has been made for the atmospheric transmission. The effect here is relatively small (only about 5% at maximum) and can be ignored relative to the error in the radiances.

Detailed investigation of the effect of radiance errors on retrieval of the microphysical properties of thin cirrus indicates that it is difficult to accurately derive an effective radius or ice water path from window 1 alone, unless an adjacent (i.e., within about 1 hour) clear-sky observation is available; however, it is still possible to retrieve IWP/r_{eff} to within 10% typically. When both windows are used, the situation improves slightly, but still inaccuracies in the window 1 radiances would only allow accurate microphysical retrievals in limited cases unless an adjacent clear-sky observation is used.

10. Investigation of other possible sources of error

A number of other quantities may conceivably affect the above results. Here we investigate the effect on the retrieval of

(i) uncertainties in the H_2O self- and foreign-broadened continuum,
(ii) the cloud top, base, and, mean temperature, and
(iii) cloud thickness.

Investigations of cases where the H_2O self-broadened continuum is changed by 20% for a typical FIRE II atmosphere reveal a difference in the downward radiance at the surface of 1 mW m^{-2} sr^{-1} $(cm^{-1})^{-1}$ at 750 cm^{-1} dropping to near zero at 1400 cm^{-1}, a behavior that mimics the differences seen between the window 1 and both-window fits for thin clouds. It should be noted that for humid atmospheres this radiance error can be as large as 10 mW m^{-2} sr^{-1} $(cm^{-1})^{-1}$. The water continuum should theoretically have only a minor effect on the retrieved values as long as the clear-sky radiances are accurately reproduced. This can still leave an error in lower-level transmittances, which in turn can affect the results. This error is an effect of the nature of the gamma correction, which, as stated above, scales the optical depths equally throughout the atmosphere. In the case of the water continuum, or indeed any far-wing or pressure-induced opacity, the absorption is proportional to the square of the density, and therefore any errors may be expected to be concentrated in the lower layers of the atmosphere. If the clouds are sufficiently high, as in the case of the cirrus clouds being investigated here, this source of error should also be negligible.

Therefore, while the effect of the water continuum in affecting these conclusions is almost certainly small, greater confidence can be placed in these results if an accurate representation of this effect can be included.

Errors in the temperature of the clouds may be more significant. Observed radiances from window 1 are almost entirely thermal, while window 2 observations are dominated by scattered solar radiation. One might therefore expect that the ratio of the two windows' signals to be affected by changing the cloud temperature and hence the "both window" fitted value for r_{eff} might be changed. Investigations were thus performed where the temperature at the cloud base and cloud top were each changed by 1, 5, and 10 K. It should be noted that

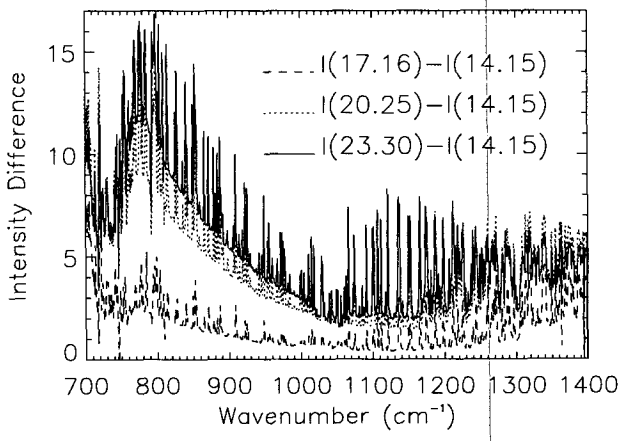

FIG. 11. A comparison of clear-sky radiances separated by 3-hour intervals as calculated from radiosonde data on 26 November 1991. The skies were clear for the 1415 and 1716 sondes, there were cirrus clouds at 2025, and there were mixed cloud layers at 2330. All times are UTC.

TABLE 6. Sensitivities of derived IWP and effective radii to cloud temperatures (percentage change per Kelvin).

Parameter being varied	Percent change in IWP (K)	Percent change in r_{eff} (K)
Cloud-top temperature: window 1 only	−2.0	−0.6
Cloud-top temperature: both windows	−2.3	−0.8
Cloud-base temperature: window 1 only	−4.0	−1.5
Cloud-base temperature: both windows	−4.0	−1.0

the cloud model assumes a linear variation in the temperature across the layer, and so changing the top or base temperature will have an affect throughout the cloud. The sensitivities to these changes are given in Table 6 in terms of percent change in IWP (or r_{eff}) per degree Kelvin.

These errors can thus be large if the temperature of the clouds is not known to within about 10 K. The larger errors are in the ice water path, however, and the above discrepancies in the effective radius derived from the two windows are not explainable with any reasonable temperature profile errors.

Experiments changing the cloud thickness have been found to result, as expected, in simply changing the ice water content by a similar factor, keeping the total ice water path the same. The effect on the effective radius was found to be at most 0.02%.

11. Comparison of results with lidar/radar measurements

Using combined lidar and radar observations, Intrieri and Feingold (1993) derived an effective radius and ice water content for the same clouds observed by the GB-HIS at FIRE on 26 November 1991. In this section these results are compared with the ones from the GB-HIS presented above.

Figure 12 shows the ice water path, the effective radius,[2] and the quotient IWP/r_{eff} as derived by the lidar/radar technique, the GB-HIS window 1, and both GB-HIS windows. The asterisks and crosses represent the 3-min-averaged GB-HIS observations, and the solid line represents results from Intrieri and Feingold (1993) averaged over approximately 1 min. The two sites were separated by ~1/4 mile (0.4 km). As might be expected from the preceding discussion, because of the different spectral regions employed and the different radiative processes occurring, the agreement is poor between the two sets of results for IWP or r_{eff}. The agreement is much better when IWP/r_{eff} is considered, especially when one remembers that the GB-HIS observations are averaged over 3-minute intervals.

12. Summary and conclusions

High-resolution Fourier transform spectrometry of the atmospheric infrared window regions is a powerful tool for investigating the radiative properties of cirrus clouds. The cloud forcing signal is, for the particles considered here, primarily a function of the ice water path and the effective radius. For the thermal emission–dominated window 1 wavelengths, the quotient IWP/r_{eff} (proportional to the optical depth) is the most important factor affecting the cloud signal. For the band II window scattering of solar radiation results in IWP/r_{eff} not being as useful a parameter.

The observed structure in the cloud spectrum in the band I window region indicates that small particles

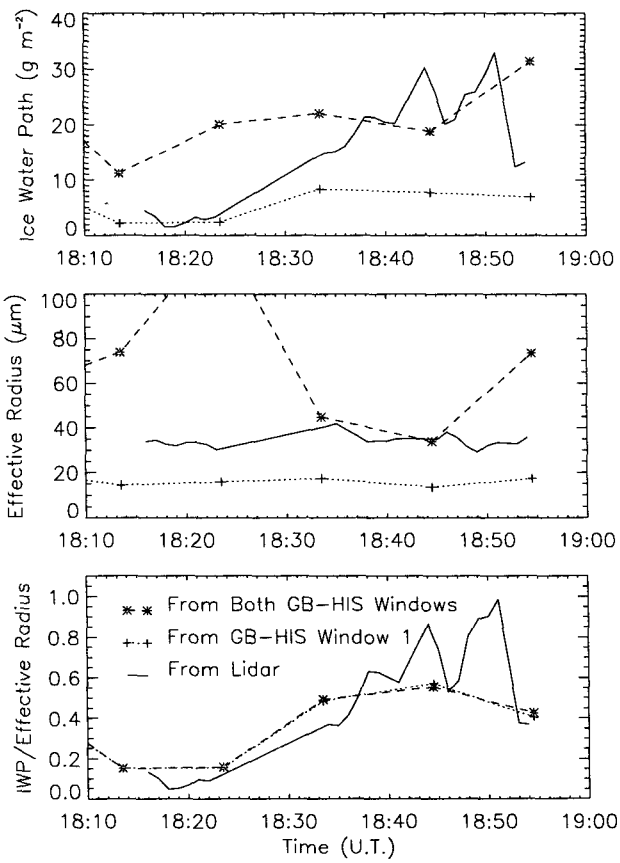

FIG. 12. A comparison between the results (effective radius, ice water path, and IWP/r_{eff}) obtained from the AERI analysis and those obtained by Intrieri and Feingold (1993) for 26 November 1991 between 1800 and 1900 UTC. The asterisks and crosses represent the 3-min averaged AERI observations for both windows and window 1, respectively, while the solid line is 1-minute averages of the lidar/radar results.

[2] The effective radius used here for the lidar/radar observations is the average over the entire cloud weighted according to the particles' total cross-sectional area at each height.

($r_{eff} \sim \lambda$) are present. This is confirmed by fitting the window 1 spectra with theoretical models. Consistent fits, in terms of cloud IWP and r_{eff}, in both windows observed by the GB-HIS (AERI) are not possible. This implies that the practice of expressing cirrus cloud microphysical properties in terms of IWP and r_{eff} for equivalent spheres is not suitable for broad spectral bands.

The discrepancy between derived cloud microphysical properties using different spectral bands may result from a variety of causes. As was shown above, two likely candidates are the nonsphericity of the cloud particles and the possibility of multimodal distributions. Most likely, the truth is a combination of these plus other factors.

The investigations into bimodality above also illustrated that the results are liable to be biased by the sensitivity of the radiance spectrum to different particle sizes. Specifically, it is apparent that the technique presented here is much more accurate in deriving the size of small particles (less than about 30 μm); larger particles tend not to affect the spectral signal as much. This insensitivity to larger particles results in large uncertainties in the derived IWP. Similarly, the lidar/radar technique of Intrieri et al. (1993) can measure particle sizes only above 30 μm, and while the IWP probably can be derived satisfactorily, the detailed spectral structure in the infrared radiances cannot be reproduced with the effective radii determined via this method. Good agreement between the GB-HIS measurements and Intrieri and Fiengold (1993) was found for the ratio of IWP/r_{eff}. Possibly the combination of lidar, radar, and spectral infrared measurements may enable a more accurate estimate of the cloud particle-size distribution.

Probably the most important effects not investigated here concern the spatial structure of cirrus clouds. The effect of vertical structure and possible separation of different particle sizes with height should be investigated soon. The effect of horizontal structure is possibly more significant; in the present work the radiative transfer problem is assumed to be essentially one dimensional. Cirrus clouds are, of course, often in the form of complex wisps of cloud, and the radiative transfer scenario is unlikely to be as simple as assumed. Furthermore, the GB-HIS integration time (about 3 min) gives time for the scene in the field of view to vary as the clouds move across the sky, complicating the situation even more. The nearly continuous dataset available from the AERI at the DOE Atmospheric Radiance Measurement (ARM) program Cloud and Radiation Testbed (CART) site near Lamont, Oklahoma, especially the cloud intensive operation periods, provide the observations needed for these future studies.

A method must thus be found to adequately describe the radiative effect of cirrus clouds with as few parameters as possible without the use of a single effective radius. In window 1 the determination of emissivities alone may suffice, but in the presence of sunlight something more is required to model the observed radiances in window 2. A compilation of inferred optical depths and asymmetry parameters may be the answer. Alternatively, it may prove to be the case that clouds can be modeled adequately by assuming the particles to be Mie scatterers but with differing (but possibly correlated) effective radii in the two windows. These possibilities will be the subject of future investigations.

It is demonstrated that consistent retrievals of the ratio IWP/r_{eff} are possible, which is proportional to cloud optical depth. An effective radius for a given spectral bandpass may thus be inferred given independent measurements of the IWP. In addition, the presence of small ice particles within the cloud is detectable using the high spectral resolution measurements.

Finally, it should be noted that, in terms of brightness temperature, the daytime signal from clouds in the band II window is much larger than that from band I, as the former is mostly due to scattered sunlight. Furthermore, the effect of the water continuum in band II is far less significant. Therefore, when the sun is above the horizon, observing in the band II window can be a very useful means of cloud detection.

Acknowledgments. The authors thank everyone who assisted in the AERI project and in particular R. G. Dedecker, H. B. Howell, and H. M. Woolf. Thanks must also go to J. M. Intrieri for supplying the data from the NOAA lidar/radar experiment. This research was supported by the NASA Grant NAG1-1177 and by the DOE Grant DE-FG-02-92ER61365.

REFERENCES

Ackerman, S. A., and R. O. Knuteson, 1993: Multiple scattering algorithm for use with line-by-line RTE models. *SPIE*, **1934**, 373–380.

——, W. L. Smith, A. D. Collard, X. L. Ma, H. E. Revercomb, and R. O. Knuteson, 1995: Cirrus cloud properties derived from high spectral resolution infrared spectrometry during FIRE II. Part II: Aircraft HIS results. *J. Atmos. Sci.*, **52**, 4246–4263.

Anderson, G. P., and J. H. Chetwynd, 1992: FASCOD3 preliminary version: FASCD3P, 57 pp. [Available from Phillips Laboratory, Hanscom AFB, MA.]

Hansen, J. E., 1971: Multiple scattering of polarized light in a planetary atmosphere. Part II: Sunlight reflected by terrestrial water clouds. *J. Atmos. Sci.*, **28**, 1400–1426.

Intrieri, J. M., and G. Feingold, 1993: Lidar and radar derived cirrus microphysical properties for the 26th November 1991 case study. Fire Cirrus Science Results, NASA Conf. Publ. 3238, 48–51.

——, G. L. Stephens, W. L. Eberhard, and T. Uttal, 1993: A method for determining cirrus cloud particle sizes using lidar and radar backscatter technique. *J. Appl. Meteor.*, **32**, 1074–1082.

Revercomb, H. E., W. L. Smith, R. O. Knuteson, F. A. Best, R. G. Dedecker, T. P. Dirkx, R. A. Herbsleb, J. F. Short, and H. B. Howell, 1993: A ground-based system for measuring atmospheric emitted radiance at high spectral resolution. *Optical Remote Sensing of the Atmosphere Technical Digest, 1993*, **5**, 82–85.

Rodgers, C. D., 1976: Retrieval of atmospheric temperature and composition from remote measurements of thermal radiation. *Rev. Geophys. Space Phys.*, **14,** 609–624.

Smith, E. V. P., and D. M. Gottlieb, 1974: Solar flux and its variations. *Space Sci. Rev.*, **16,** 771–802.

Smith, W. L., X. L. Ma, S. A. Ackerman, H. E. Revercomb, and R. O. Knuteson, 1993: Remote sensing cloud properties from high spectral resolution infrared observations. *J. Atmos. Sci.*, **50,** 1708–1720.

——, H. E. Revercomb, S. A. Ackerman, F. A. Best, A. D. Collard, R. G. Dedecker, H. B. Howell, H. Huang, R. O. Knuteson, X. Ma, and H. M. Woolf, 1995: Cirrus cloud properties derived from high spectral resolution infrared spectroscopy during FIRE II. Part I: The high resolution interferometer sounder (HIS) systems. *J. Atmos. Sci.*, **52,** 4238–4245.

Uttal, T., J. M. Intrieri, T. P. Ackerman, W. L. Eberhard, and E. Clothiaux, 1995: Cloud boundary statistics during FIRE II. *J. Atmos. Sci.*, **52,** 4276–4284.

Wiscombe, W., 1976a: Extension of the doubling model to inhomogeneous sources. *J. Quant. Spectrosc. Radiat. Transfer,* **16,** 477–489.

——, 1976b: On initialization, error and flux conservation in the doubling method. *J. Quant. Spectrosc. Radiat. Transfer,* **16,** 637–658.